Electronic Supplementary Material (ESI) for Journal of Materials Chemistry A.

Supporting Information

Engineering Crystallinity of MoS_2 Monolayers for Highly Efficient Solar Hydrogen Production

Xiao Hai, Wei Zhou, Kun Chang, Hong Pang, Huimin Liu, Li Shi, Fumihiko Ichihara, and Jinhua Ye**

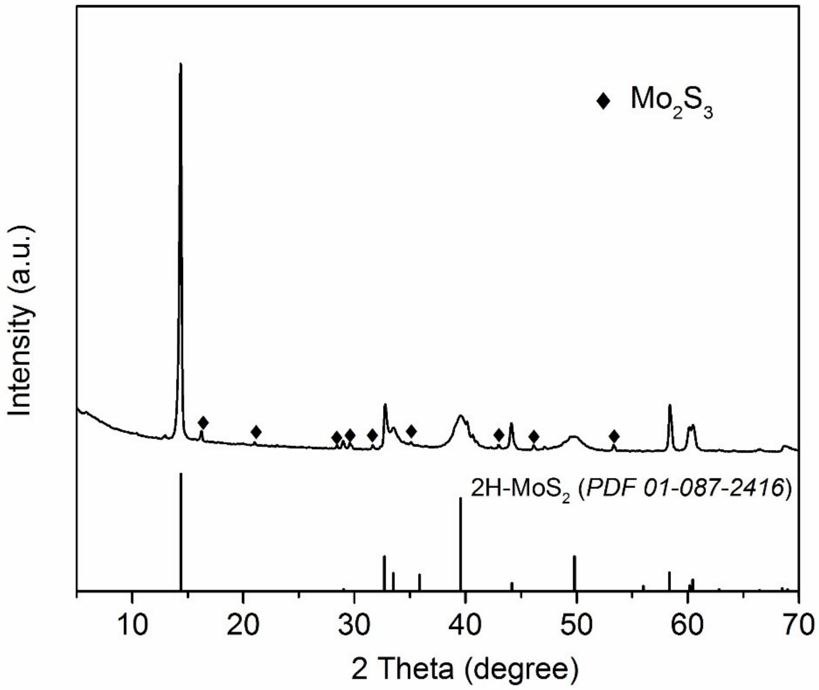

Fig. S1 XRD pattern of the prepared bulk MoS_2 crystal with calcination temperature at 1200°C. There existed impurity phase (Mo_2S_3) when the calcination temperature reached as high as 1200°C.

Note: It is known that MoS_2 can be generated by thermal decomposition of $(NH_4)_2MoS_4$, which the salt decomposes in two distinct steps as following equations[1]:

$(NH_4)_2MoS_4 \rightarrow 2NH_3\uparrow + H_2S\uparrow + MoS_3$ (1)

$MoS_3 \rightarrow MoS_2 + S\uparrow$ (2)

The first step (equation, eq. 1) involves the decomposition to the MoS_3 and the released NH_3 and H_2S gas, and the second step (eq. 2) the decomposition of the MoS_3 to the MoS_2 and elemental sulfur. It is known that the decomposition temperature of MoS_3 is over 335 °C[1]. Thus, our controllable experimental temperature is in the range from 400°C to 1100°C.

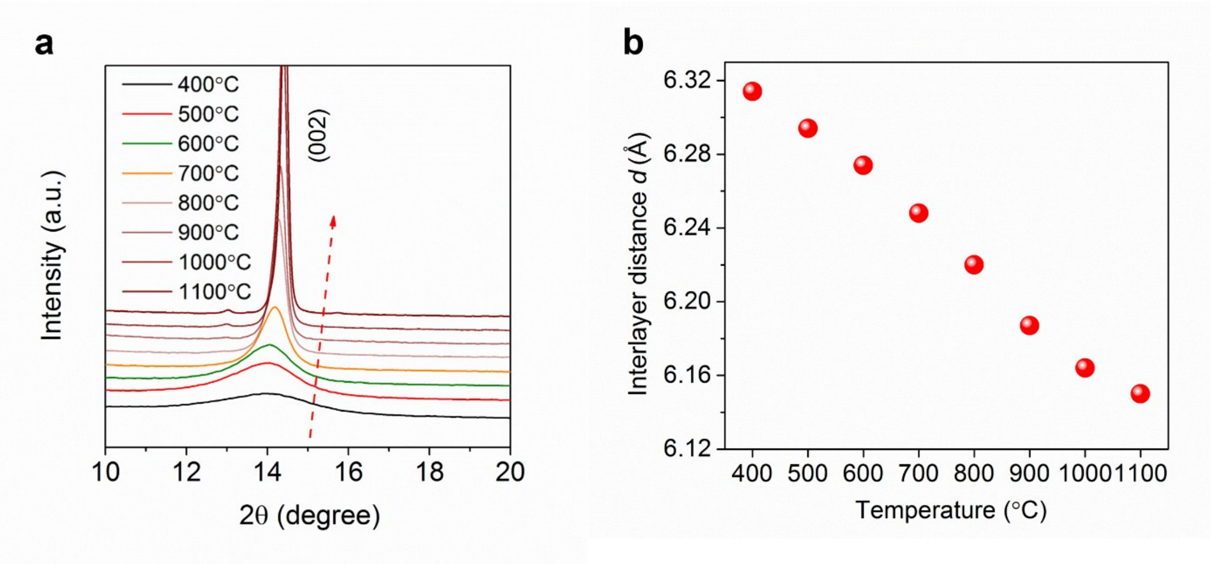

Fig. S2 (a) Enlarged view of the (002) peak. The position of (002) peak monotonously shifts toward higher angle with the increase of calcination temperature. (b) The calculated interlayer distance from the position of (002) peak.

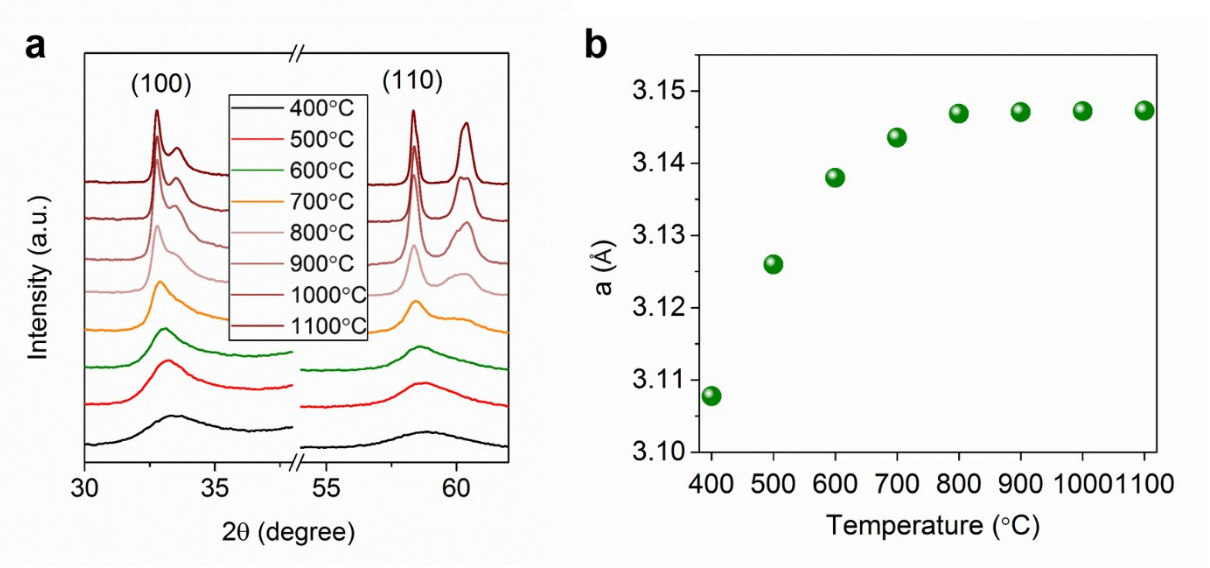

Fig. S3 (a) Enlarged view of the (100) and (110) peaks. (b) The calculated in-plane lattice parameter from the position of (110) peak.

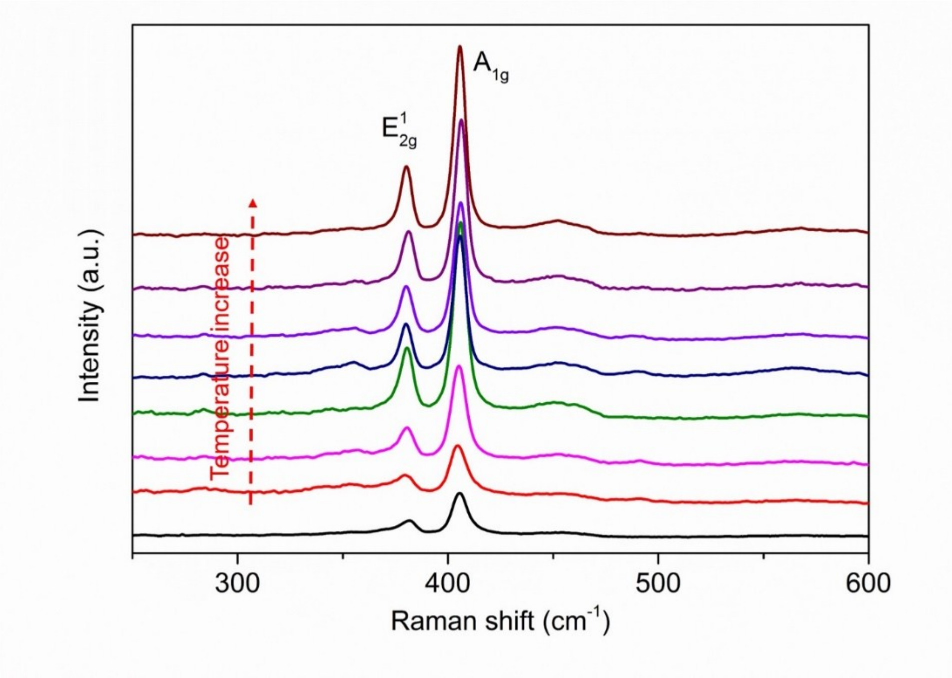

Fig. S4 Raman spectra of the as-prepared differently crystalline bulk MoS_2 crystals. Raman spectra further confirmed the 2H-phase structure by the appearance of two distinct peaks at 380 cm^{-1} and 406 cm^{-1}, which correspond to the in-plane vibration (E_{2g}^1) and out-of-plane mode (A_{1g}), respectively[2].

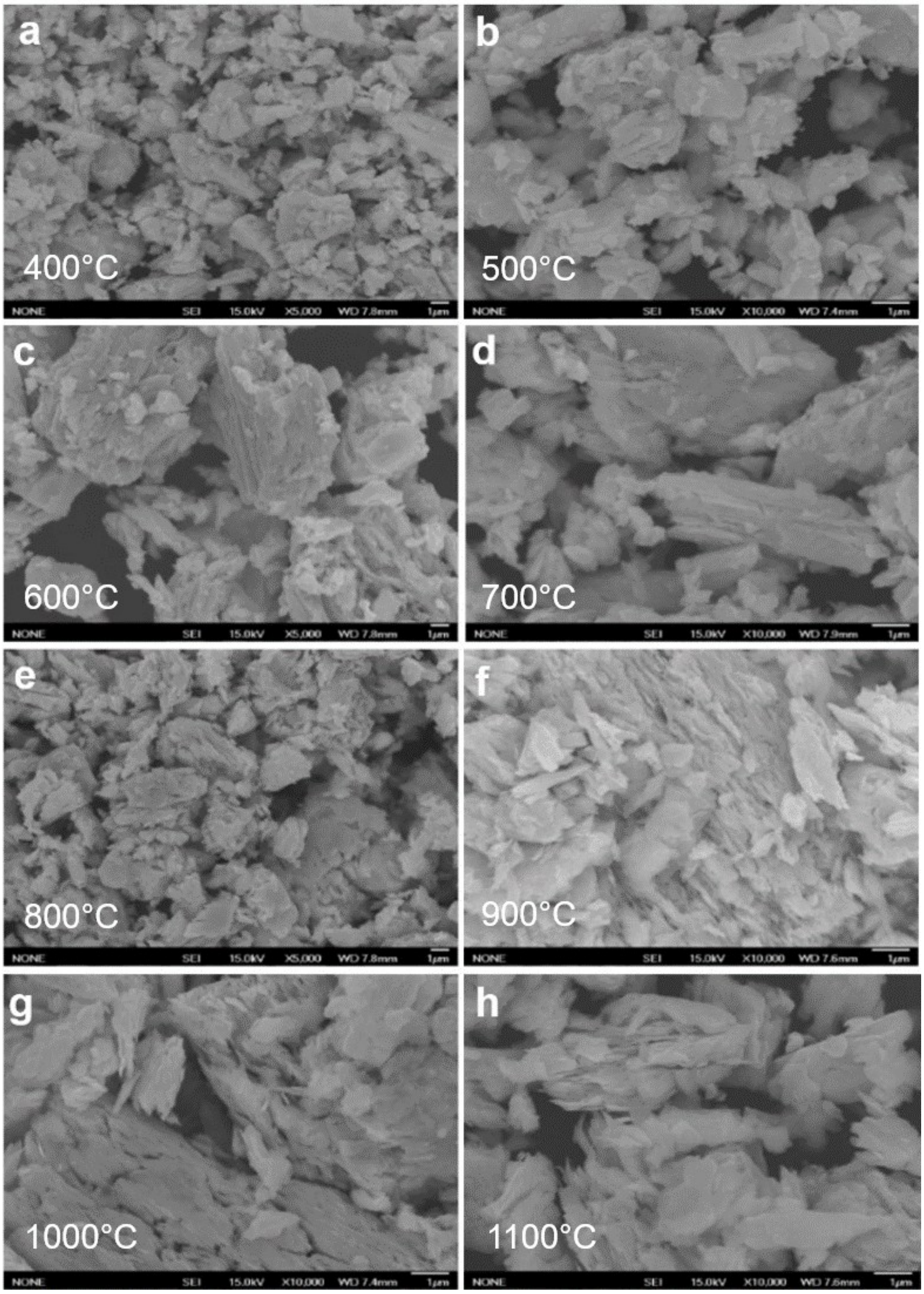

Fig. S5 (a-h) SEM images of differently crystalline bulk MoS_2 crystals in the range of 400°C to 1100°C with per 100°C.

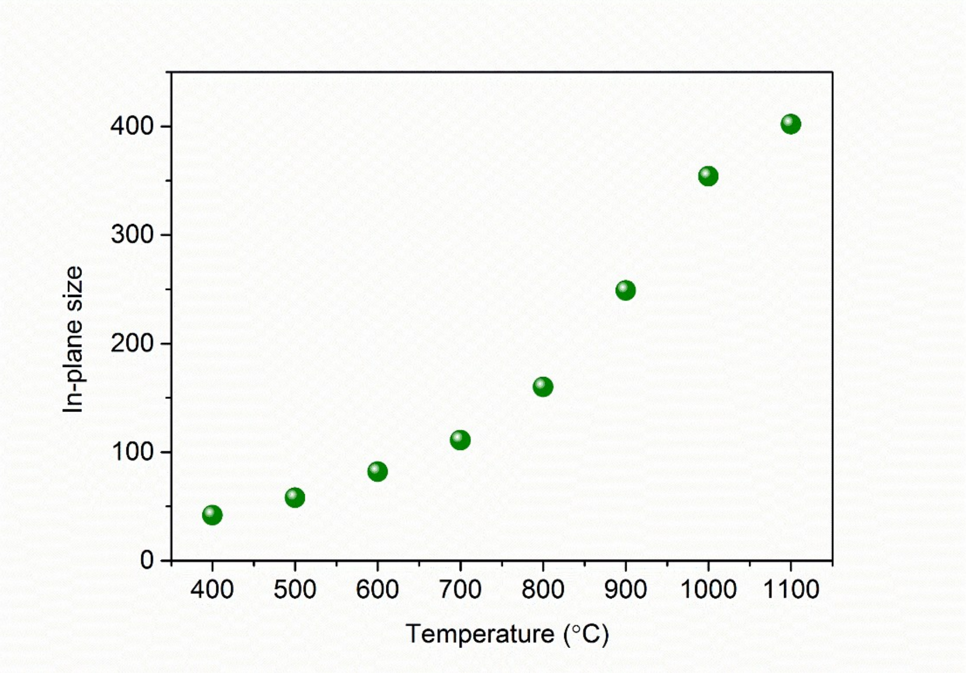

Fig. S6 In-plane size calculated by the full-width at half-maximum of the (110) reflection in the XRD patterns.

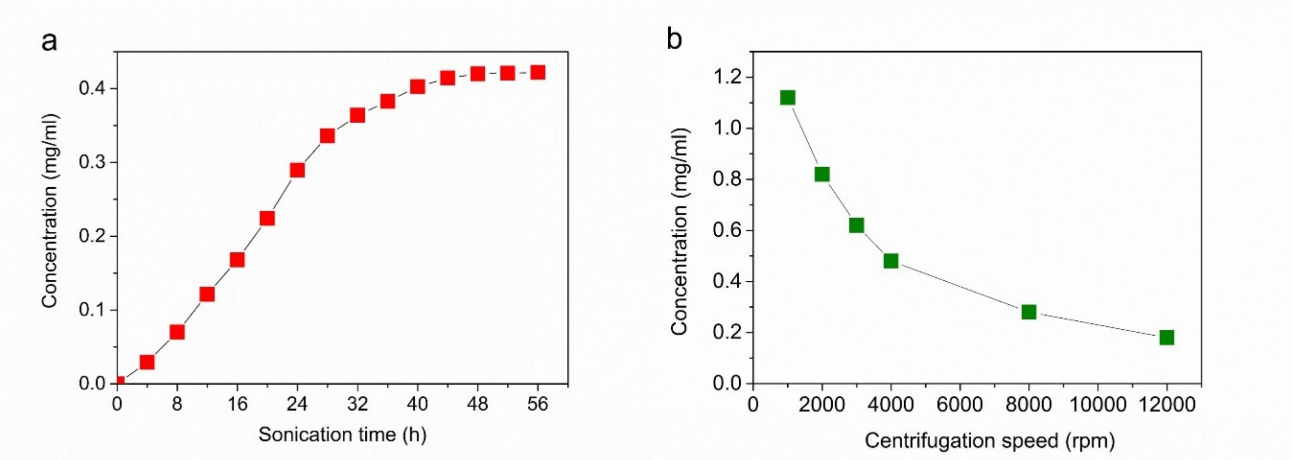

Fig. S7 Optimization of 800-MoS_2 dispersions in ethanol. (a) Concentration of the obtained nanosheets after sonication for different times. The concentration of exfoliated MoS_2 nanosheets was quickly increased in the first 48 hours and slowed down, reaching the maximum in exfoliation. So, we sonicated the bulk precursors in ethanol solvent for 48 hours. (b) Concentration of nanosheets after centrifugation at different rates. The obtained dispersions centrifuged at different rates were studied by AFM to check the exfoliated nanosheets. We found that the best centrifugation process was first centrifuged at 2000 rpm (RCF 760 g) for 1 hour, the top 2/3 portions of the supernatants were carefully collected by pipette. The obtained supernatants were added into a new glass vial and sonicated again for another 4 hours. Then, the monolayer dispersions were collected by pipette followed by another centrifugation of the supernatants at 4000 rpm (RCF 3020 g) for 1 hour.

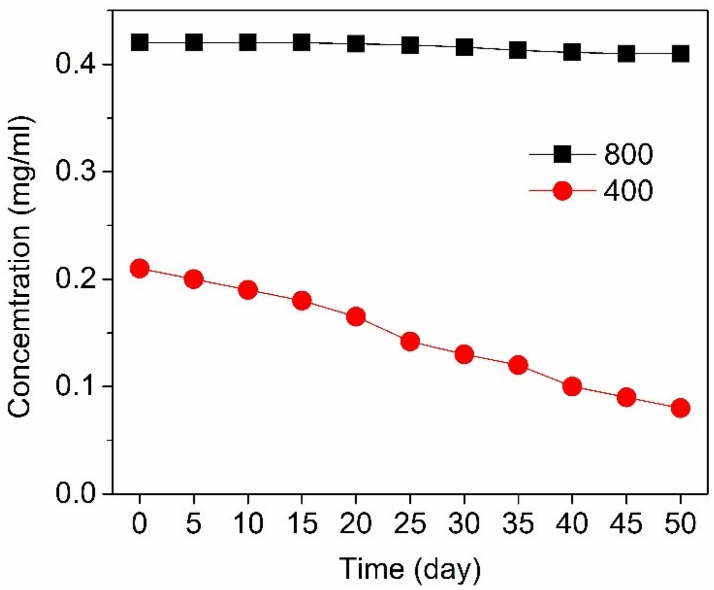

Fig. S8 Comparison of concentration retention as a function of time for 400- and 800-MoS_2 monolayers. The lowly crystalline MoS_2 monolayer exhibited a less stability compared with the highly crystalline counterpart.

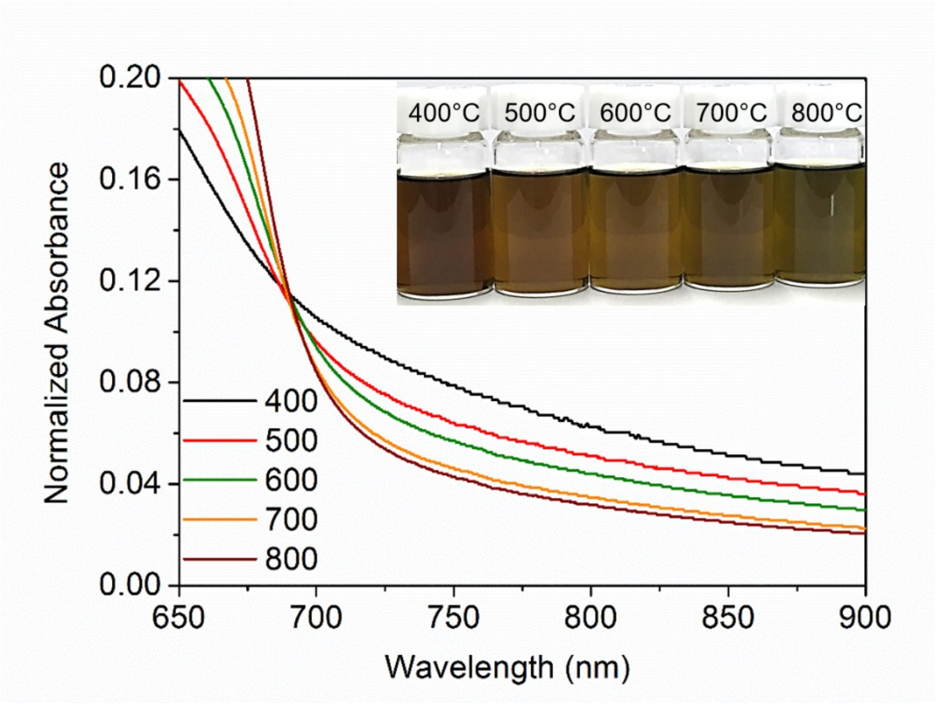

Fig. S9 Tail absorption of the differently crystalline monolayer MoS_2 dispersions, inset is the corresponding photograph.

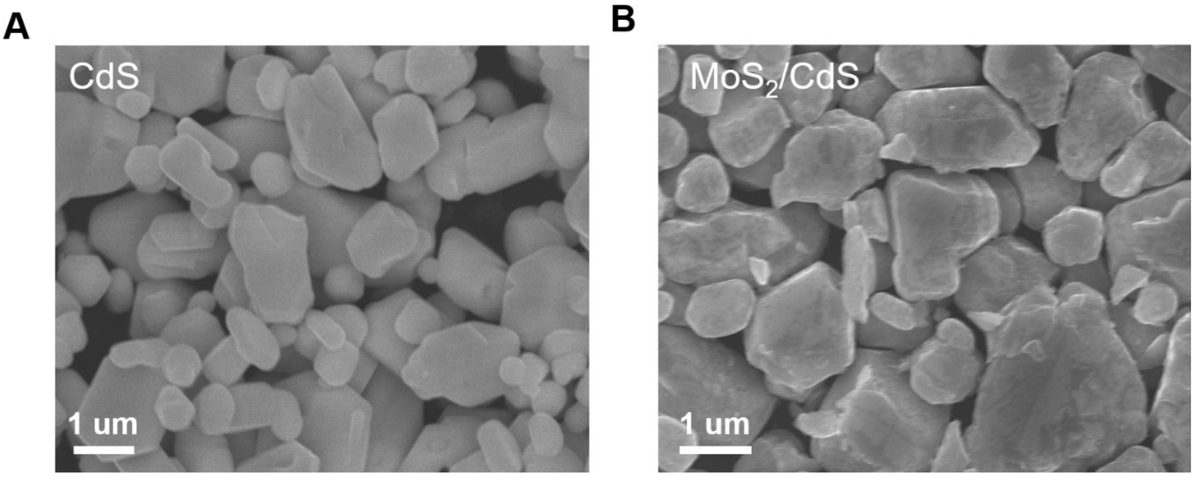

Figure. S10 SEM images of the commercial CdS before (A) and after (B) loaded 2.0 wt% of monolayer MoS_2 nanosheets.

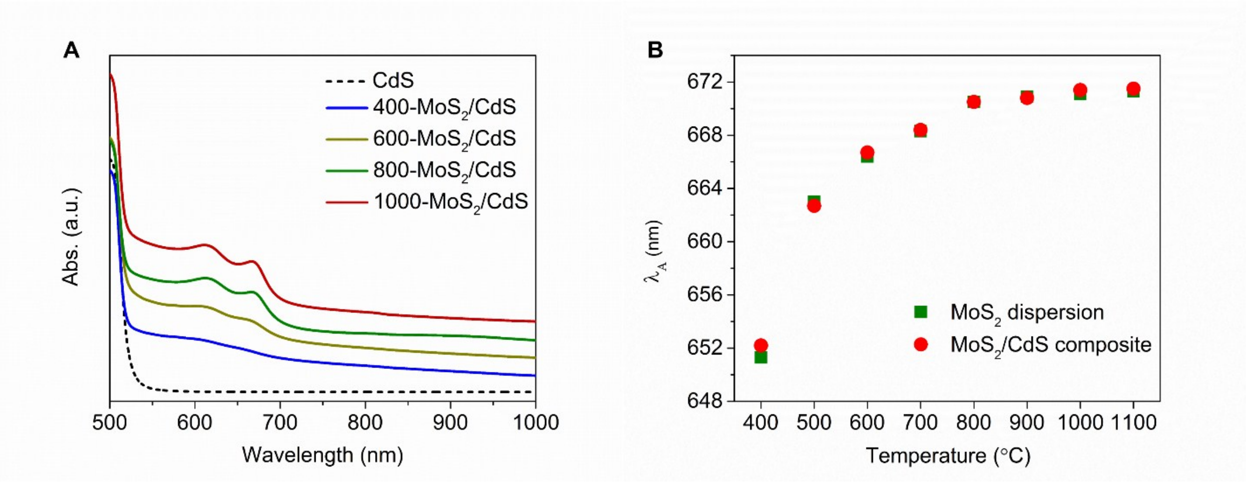

Fig. S11 (A) UV-vis-NIR absorption spectra of pure CdS and the corresponding MoS_2/CdS composites. Fortunately, the absorption near A-exciton of MoS_2 is not affected due to the suitable band structure of CdS, leading to an accurate access of the absorption information regarding peak A. (B) Comparison of λ_A derived from absorption spectra of the MoS_2/CdS composites and monolayer MoS_2 dispersions.

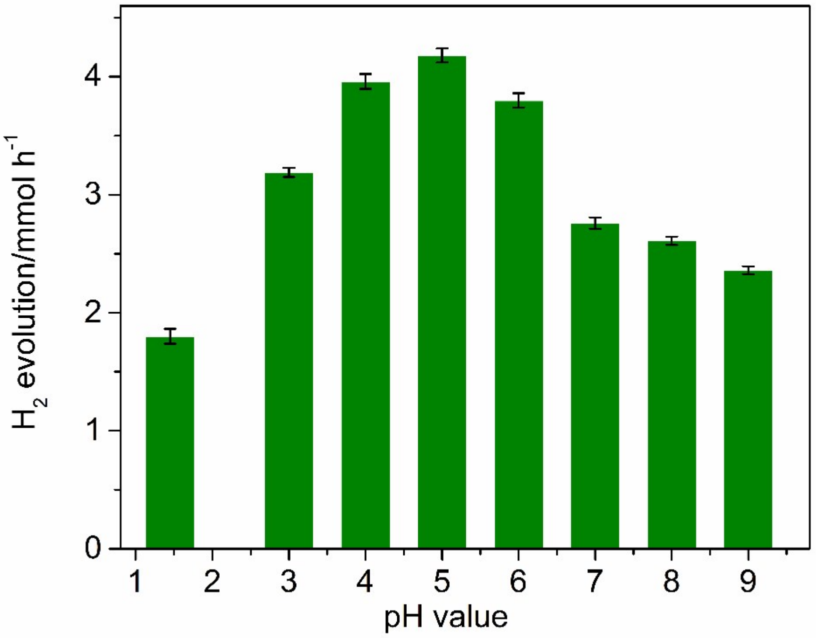

Fig. S12 Photocatalytic H_2 evolution activities of the 800-MoS_2/CdS composite versus pH value. Light source: 300-W Xe lamp with a L42 cut-off, λ > 420 nm; Reaction solution: 300 mL lactic acid solution (30 vol. %, pH=1.45), pH value was adjusted by NaOH; Catalyst: 200 mg, cocatalyst: 2wt %. Considering that the ΔG_{H*} of MoS_2 active sites is slightly more than zero, the rate determining step in HER is the adsorption step. Although an acidic environment with an appropriate amount of H^+ favors HER performance, the photoharvester CdS is not stable in a strongly acidic environment. To obtain the optimum parameters for efficient HER, we systematically investigated the pH effect on photocatalytic H_2 activity of the MoS_2/CdS composite.

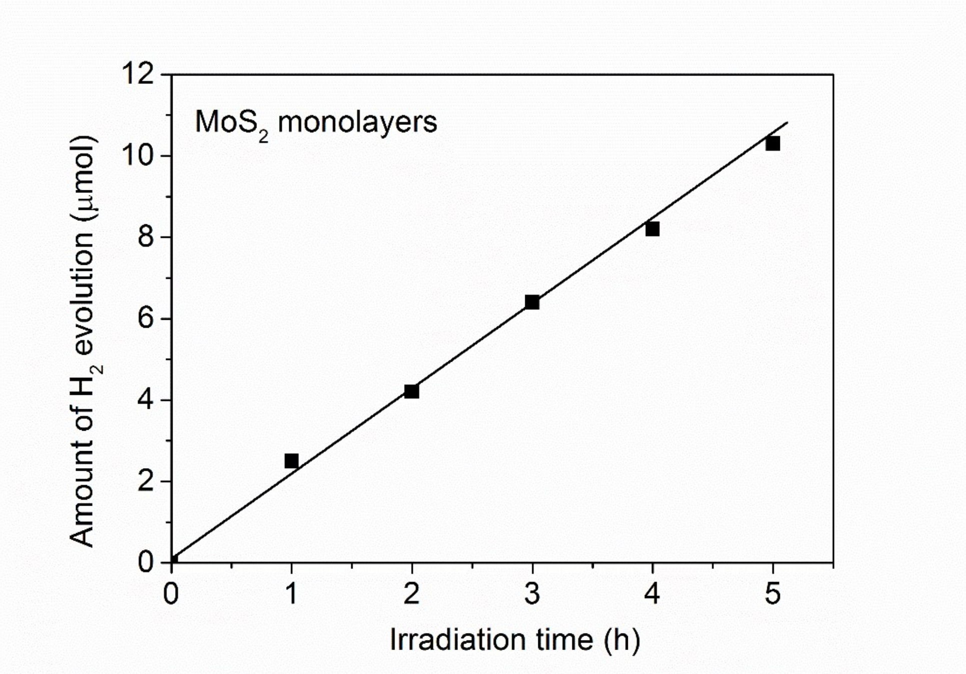

Fig. S13 Photocatalytic H_2 evolution activities of bare 800-MoS$_2$ monolayers under visible light irradiation. Light source: 300-W Xe lamp with a L42 cut-off, $\lambda > 420$ nm; Reaction solution: 300 mL sodium lactate solution (30 vol. % lactic acid adjusted by NaOH, pH=5.0), Catalyst: 4 mg.

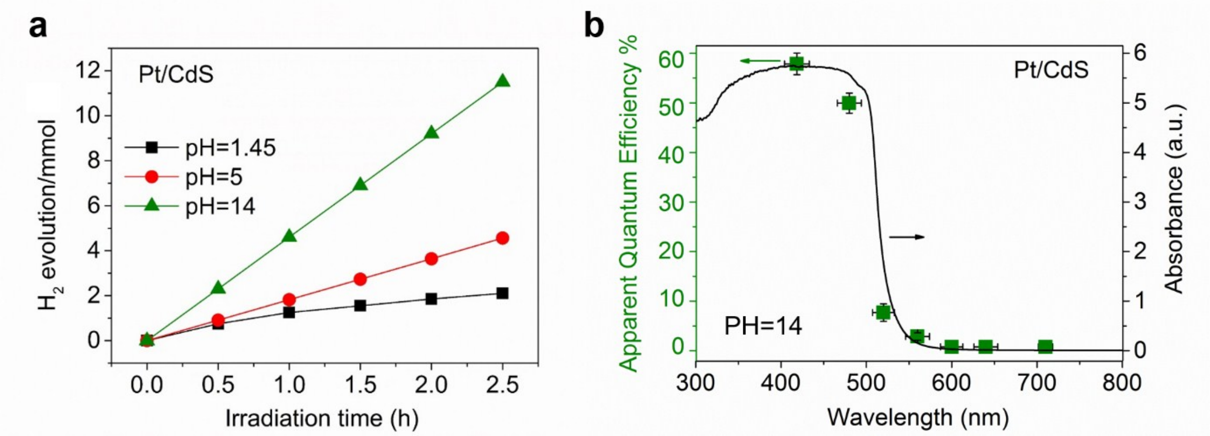

Fig. S14 (a) Photocatalytic H_2 evolution activities of Pt/CdS under visible light irradiation. Light source: 300-W Xe lamp with a L42 cut-off, λ > 420 nm; Reaction solution: 300 mL lactic acid solution (30 vol. %, pH=1.45), 300 mL sodium lactate solution (30 vol. % lactic acid adjusted by NaOH, pH=5.0), 300 mL Na_2S-Na_2SO_3 solution (pH=14); Catalyst: 200 mg; cocatalyst: 0.65 wt%[3]. (b) Wavelength-dependent apparent quantum efficiency of H_2 evolution from the Pt/CdS composite in 300 mL Na_2S-Na_2SO_3 solution.

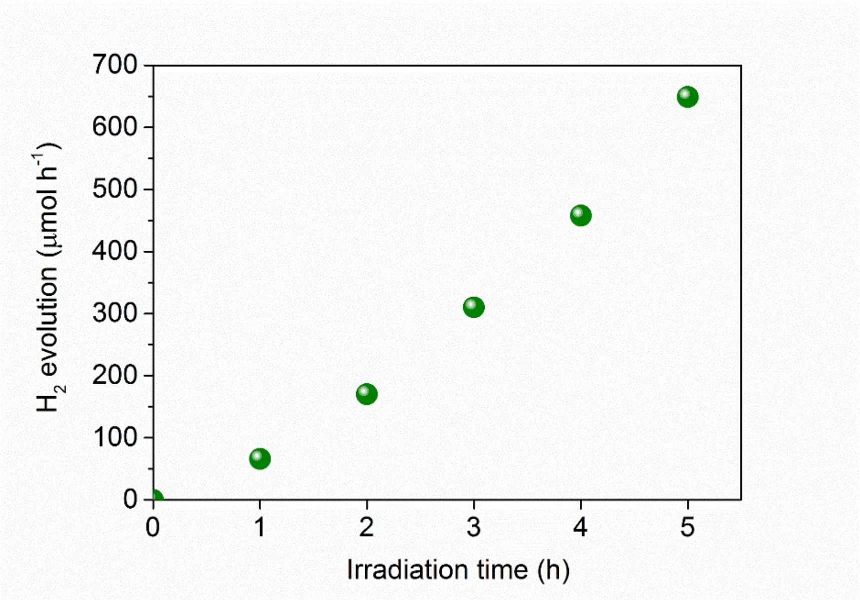

Fig. S15 The photocatalytic hydrogen evolution activity of bare CdS. Light source: 300-W Xe lamp with a L42 cut-off, λ > 420 nm; Reaction solution: 300 mL sodium lactate solution (30 vol. % lactic acid adjusted by NaOH, pH=5.0), Catalyst: 200 mg.

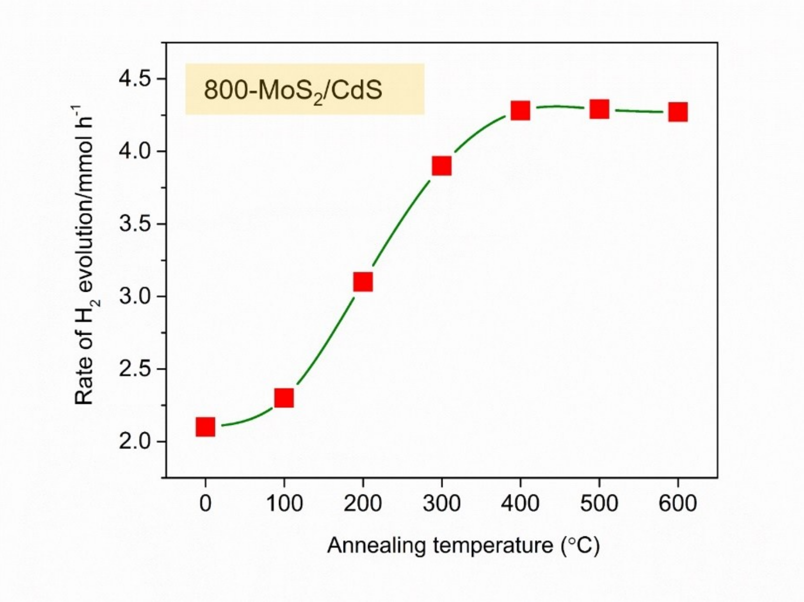

Fig. S16 Photocatalytic H_2 evolution activities of the 800-MoS$_2$/CdS composite with different heat treatment temperature. Light source: 300-W Xe lamp with a L42 cut-off, $\lambda > 420$ nm; Reaction solution: 300 mL sodium lactate solution (30 vol. % lactic acid adjusted by NaOH, pH~5.0); Catalyst: 200 mg, cocatalyst: 2.0 wt %.

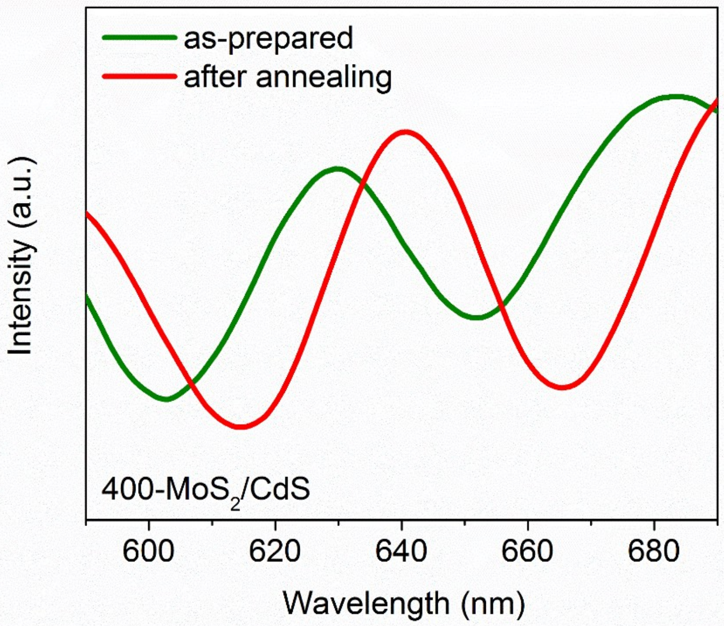

Fig. S17 Second derivative of the absorption spectra for 400-MoS_2/CdS composite before and after annealing at 600 °C.

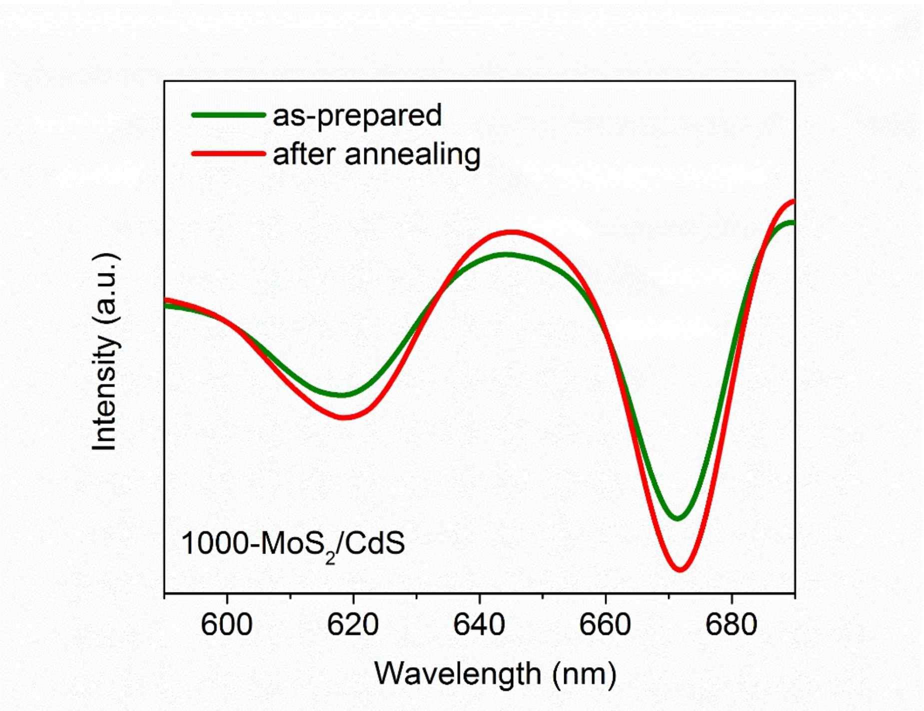

Fig. S18 Second derivative of the absorption spectra for 1000-MoS$_2$/CdS composite before and after annealing at 600 °C.

Table S1. Exfoliability and stability test of crystallinity-dependent MoS_2.

Temperature (°C)	Concentration (mg mL^{-1})	Monolayer yield	Zeta potential (mV)
400	0.18	9.0%	-20.6 ± 5.9
500	0.23	11.5%	-28.1 ± 4.6
600	0.31	15.5%	-35.8 ± 4.9
700	0.39	19.5%	-42.2 ± 4.6
800	0.42	21.0%	-50.7 ± 4.7
900	0.36	18.0%	-52.3 ± 4.0
1000	0.27	13.5%	-53.1 ± 3.6
1100	0.22	11.0%	-53.3 ± 4.1

References

(1) T. P. Prasad, E. Diemann, A. Muller, *J Inorg Nucl Chem* **1973**, 35, 1895.

(2) C. Lee, H. Yan, L. E. Brus, T. F. Heinz, J. Hone, S. Ryu, *ACS nano* **2010**, 4, 2695.

(3) K. Chang, M. Li, T. Wang, S. X. Ouyang, P. Li, L. Q. Liu, J. H. Ye, *Adv. Energy. Mater.* **2015**, 5, 1402279.